Hindawi
Geofluids
Volume 2023, Article ID 8528359, 15 pages
https://doi.org/10.1155/2023/8528359

Research Article

Methane Adsorption in Anthracite Coal under Different Pressures and Temperatures—A Study Combining Isothermal Adsorption and Molecular Simulation

Tieya Jing, Jian Zhang, Mingyu Zhu, Wentao Zhao, Juan Zhou, and Yulong Yin

Beijing Key Laboratory of CO_2 Capture and Treatment, China Huaneng Clean Energy Research Institute, Beijing 102209, China

Correspondence should be addressed to Mingyu Zhu; 18133801859@163.com

Received 23 June 2022; Revised 24 August 2022; Accepted 1 October 2022; Published 10 May 2023

Academic Editor: Yong Li

In situ gas content is an important parameter associating coalbed methane, while the influence of pressure and temperature on methane adsorption and desorption still needs to be revealed. In this study, the molecular structure and methane adsorption capacity of anthracite coal collected from Diandong Coalfield (China) were studied based on ^{13}C nuclear magnetic resonance (^{13}C NMR), Fourier transform infrared spectroscopy (FT-IR), and methane isothermal adsorption experiment. The results show that the carbon skeleton of coal sample is mainly composed by aromatic carbon (72%), followed by aliphatic carbon structure (14.2%). Carbons connected to the oxygen atoms contribute 13.7% of the total carbons in coal molecule, and the oxygen atoms are mainly in the form of carbonyl. The 2-dimension structure and 3-dimension molecular structure of coal sample was also reconstructed. The average chemical formula of the coal molecule is $C_{200}H_{133}O_{21}N_3$. The experimental methane adsorption isothermal data of the coal sample under different temperatures shows that with increasing the temperature, the methane adsorption amount at each pressure decreases obviously. At 7 MPa and 20°C, the methane adsorption amount of the coal sample is 28.5 cm^3/g. Comparably, at 100°C and 7 MPa, the methane adsorption amount is only 15.9 cm^3/g, decreasing by 44%. In mesopores, temperature has stronger influence on methane adsorption under higher pressure than that of lower pressure. On the contrary, in micropores, temperature has weaker effects on methane adsorption at higher pressure than that at lower pressure. The results can be beneficial for understanding methane adsorption characteristics of deep coal.

1. Introduction

Coalbed methane (CBM) is clean energy and has been widely extracted and utilized with huge potential in China [1–5]. The accumulation mechanism of CBM is quite different from other types of natural gas as CBM is mainly stored as absorbed state [6–8]. Thus, methane adsorption mechanism in coal is considered to be one of the most important factors to realize CBM production [9–12]. In previous studies, it was found that the adsorption behavior of methane in coal is caused by intermolecular interaction forces between methane molecules and coal matrix [11, 13]. In addition, the coal maturity, composition, pore structure, pressure and temperature all have effect on the methane adsorption capacity [8, 14–18]. However, the pore system in coal is complex, and this makes the methane adsorption mechanism in coal is still unclear [19–21].

Methane adsorption isothermal experiment (gravimetric method or volumetric method) is commonly used to test the methane adsorption capacity of coal reservoir [15, 22]. The adsorption behavior has been widely studied under different pressure and temperature conditions [23, 24]. It was found that with increasing methane pressure, the adsorption capacity increases, which can be simulated by the Langmuir equation [23, 25, 26]. Besides, with increasing temperature, the methane adsorption capacity decreases. When the

vitrinite reflectance of the coal sample increases from 0.5% to 3.7%, the methane adsorption capacity decreases firstly and then increases [17, 24, 27]. In general, the anthracite coals have strong adsorption capacities [24, 28]. The in-situ CBM contents in many anthracite coalfields were found much higher than other coal seam [29].

Molecular simulation has been applied in studying the methane adsorption mechanism as molecule simulation could provide molecule-scale information about the methane adsorption behavior in coal [30–32]. The density distribution of adsorbed methane, the location of the adsorbed methane, and the methane adsorption behavior of different size pores in coal can be directly provided by the molecule simulation [13, 33, 34]. Therefore, the molecule simulation has received extensive attention in coalbed methane studies. The graphite-slit pore models are used to represent the adsorption behavior of methane in slit pores [13]. However, the coal molecule structure is significantly different from graphite [32, 35].

In the studies of CBM, it is important to evaluate the in situ methane content in coal. As the depth of the coal is different in different coalfields, the pressure and temperature of underground coal seams are different. The increase of burial depth of the coal seam can lead to temperature and pressure increment. However, it is unclear how temperature and pressure affect methane adsorption behavior. In this study, the influence of pressure and temperature on methane adsorption behavior is investigated by both physical experiments and molecular simulation methods.

2. Methodology

2.1. Samples. The coal samples used in this study are collected from No. 2 coal seams in Yuwang coal mine in East Yunnan (Diandong coalfield), China. Yuwang coal mine is an underground coal mine with high gas content. The average thickness of No. 2 coal seams is 1.13 m. The vitrinite reflectance of these coal samples is about 2.4%. The ash content of the coal sample is 23.66% and the volatile content is 9.99% under air-dry basis.

2.2. Experiments

2.2.1. ^{13}C Nuclear Magnetic Resonance (^{13}C NMR). The ^{13}C NMR experiment was conducted by JNM-ECZ600R in Nuclear Magnetic Resonance Center of Tsinghua University. The powder coal samples were used and resonance frequency was set to 150 MHz. During the experiment, the mass frequency was set to 12 kHz with the total scan time of one hour (1200 times) [36].

2.2.2. Fourier Transform Infrared Spectroscopy (FT-IR). When performing the FT-IR experiment, PerkinElmer spectrum (Frontier FT-IR) was used. About 2 g powder coal samples were used in the experiment. Before the experiment, atmospheric correction was performed. The scanning range was set from 450 cm^{-1} to 4000 cm^{-1}. The scanning speed is 0.2 s^{-1}. The analysis of the FT-IR is based on the previous study [37].

2.2.3. Methane Isothermal Adsorption Experiment. The Methane isothermal adsorption experiment was performed in Unconventional Natural Gas Laboratory, China University of Mining and Technology, Beijing. Before the experiment, the Yuwang coal samples were pulverized to about 60-80 mesh and were dried at 80°C for 24 hours. Methane adsorption experiments were carried out by the 3H-2000PH methane adsorption instrument by volumetric method. For the instrument, the pressure can be set to as high as 690 bar (69 MPa).

2.3. Simulation Methods

2.3.1. Coal Molecule Reconstruction. The reconstruction process of coal molecular model contains several steps. Firstly, the molecular information of the model was obtained by statistical analysis of the experimental data such as industrial analysis, elemental analysis, ^{13}C NMR, and FT-IR. Then, the initial model satisfying the structural information is drawn by ACD/ChemSketch. After that, the ^{13}C NMR of initial model was calculated and compared to the experimental data. The initial model wall was corrected based on the comparing results to obtain the objective two-dimensional model structure. The two-dimensional model will be imported for model optimization to obtain the three-dimensional model with the lowest energy configuration. Finally, the periodic boundary is added to truly restore the microstructure of coal samples. The details of the molecule reconstruction process can be also seen in previous studies [38, 39].

2.3.2. Simulation of Methane Adsorption in Coal. The methane adsorption in coal is physical adsorption, and the interaction forces are mainly Van de Waals forces. In the simulation, the Van de Waals forces are calculated by Lennard-Jones potential energy function. The simulation was carried out at different temperature and different pressure. The maximum pressure is 7 MPa. The temperature and pressure conditions are set according to the experimental conditions.

3. Results

3.1. Results of ^{13}C NMR. According to the previous studies, the ^{13}C NMR spectrum of the Yuwang coal sample can be divided into four parts: aliphatic carbon peaks (chemical shift = 0 − 60 ppm), ether oxygen carbon peaks (chemical shift = 60 − 90 ppm), aromatic carbon peaks (chemical shift = 100 − 165 ppm), and carbonyl and carboxyl carbon peaks (chemical shift = 165 − 250 ppm) [40, 41]. Peak fitting of the ^{13}C NMR spectrum was performed by using the software origin. The fitting results were shown in Table 1 and Figure 1.

According to the peak fitting results, the carbon skeleton structure of YW coal sample is mainly composed by aromatic carbon structure (72%), followed by aliphatic carbon structure (14.2%). Carbons connected to the oxygen atoms contribute 13.7% of the total carbons in coal molecule. In addition, the aromatic carbon structure is mainly composed by benzene rings and naphthalene rings. There are less anthracene rings and phenanthrene rings. The structures of

Table 1: ^{13}C NMR peak attribution and relative content of YW samples.

Serial number	Peak type	Half peak width (ppm)	Chemical shift (ppm)	Relative area (%)	Peak position attribution
1	Gaussian	8.0	19	2.4	Aromatic methyl
2	Gaussian	11.2	32	3.51	Methylene, methylene
3	Gaussian	14.4	45	8.3	Seasonal carbon
4	Gaussian	4.1	107	0.5	Protonated aromatic carbon
5	Gaussian	15.4	126	63.7	Bridged aromatic carbon
6	Gaussian	9.3	141	7.8	Alkyl substituted aromatic carbon
7	Gaussian	9.5	200	5.2	Carboxyl carbon
8	Gaussian	7.4	208	5.5	Carbonyl carbon
9	Gaussian	10.0	215	3.0	Carbonyl carbon

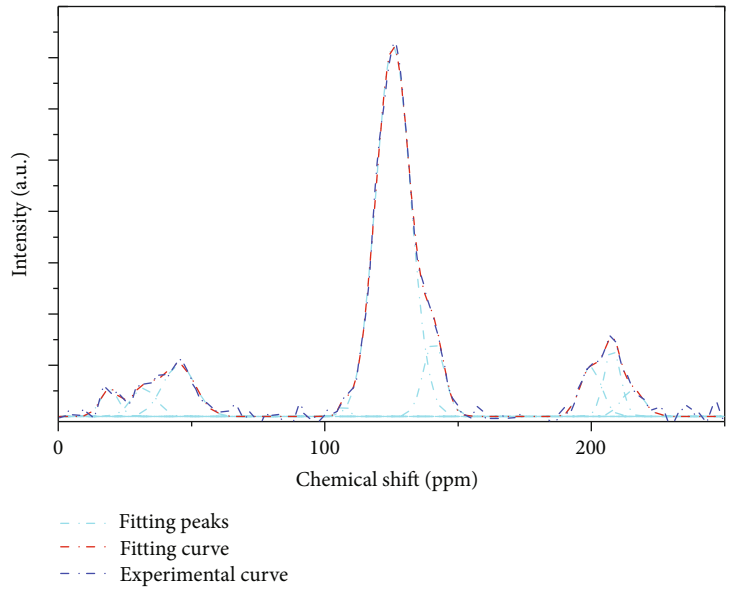

Figure 1: ^{13}C NMR data of the YW coal samples with the peak fitting results.

aliphatic carbon on the side chain are mainly composed by methyl and methylene. The oxygen-containing functional groups are mainly ether bonds. According to elemental analysis and ^{13}C NMR data, the aromaticity rate is 74.5%, and the total carbon in coal molecular structure unit is 200. The ratio of benzene : naphthalene : anthracene : phenanthrene : pentacene in YW sample is 5 : 5 : 3 : 0 : 2 (Table 2).

3.2. Results of FT-IR. The peak fitting results of FT-IR are shown in Figure 2. The assignment of each peaks are according to Tables 3–6. The region between 2800 and 3000 cm^{-1} of FT-IR spectrum is the aliphatic carbon region. The infrared spectrum of this region shows that the side chain alkyl is mainly methylene and there is a small amount of methyl (Table 6).

3.3. Coal Molecular Construction. The ^{13}C NMR and FT-IR data are used to reconstruct the chemical molecular structure of anthracite, and the average chemical formula of the anthracite coal molecule is $C_{200}H_{133}O_{21}N_3$, as shown in Figure 3(a). In addition, it can be seen that the oxygen atoms are mainly in the form of carbonyl groups, which can be also found from the ^{13}C NMR spectrum. The nitrogen atoms are in the form of pyrrole rings. After annealing and geometrically optimizing the 2D molecule, it can be found that the aliphatic side chain is obviously elongated and the aromatic carbon structure is distorted, as shown in Figures 3(b) and 3(c). Simultaneously, 14 optimized anthracite molecules put into the unit cell to construct a 3D structure of anthracite coal as shown in Figure 3(d). The size of the 3D molecular structure is 3.345 nm × 3.345 nm × 3.345 nm.

Table 2: Forms of aromatic carbon with different molecular configurations of coal samples.

Existing forms of aromatic carbon	Numbers
Benzene	5
Naphthalene	5
Anthracene	3
Phenanthrene	0
Pentacene	2
Pyrrole	3

3.4. Methane Adsorption Isothermal Data. Figure 4 illustrates the experimental methane adsorption isothermal data

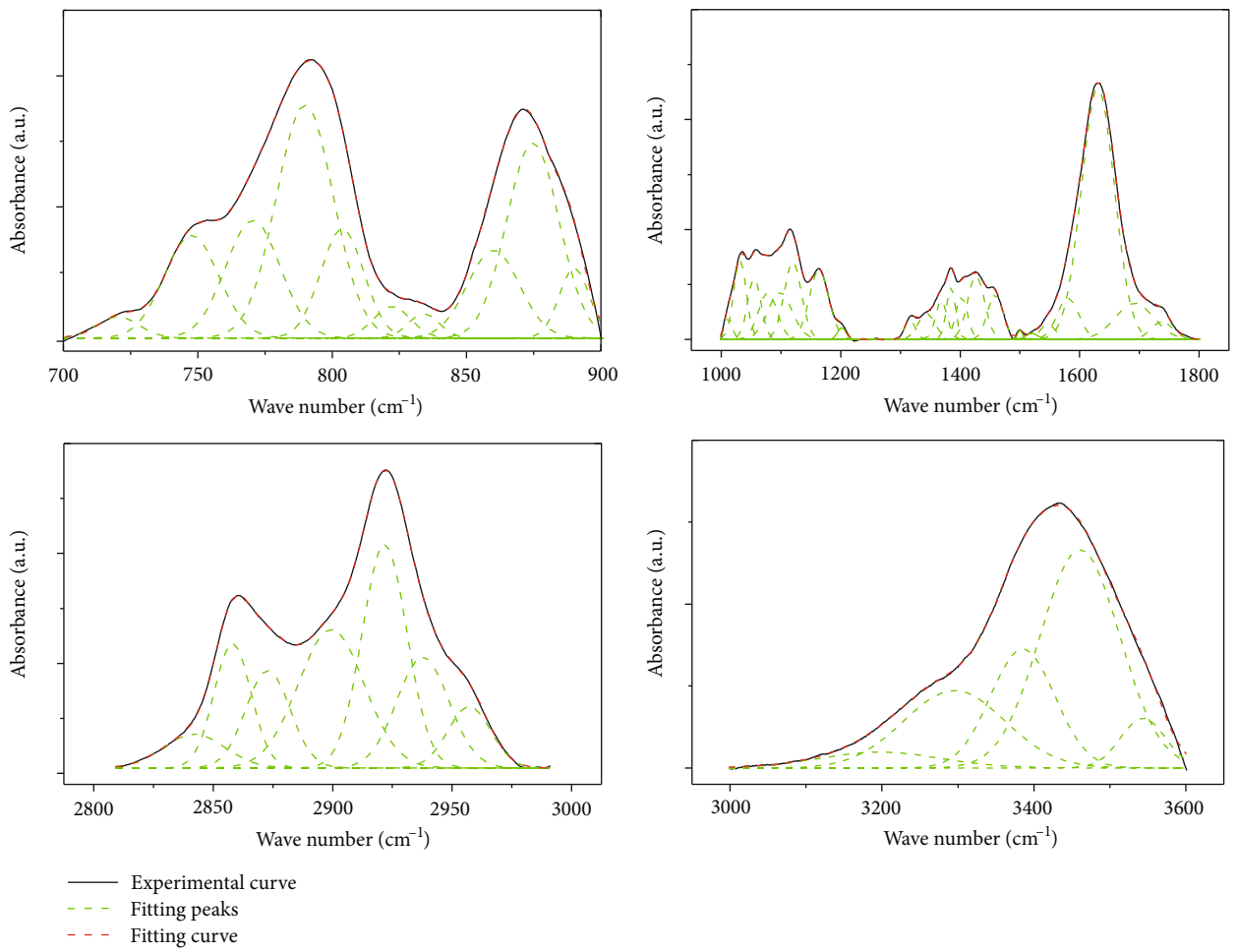

Figure 2: The peak fitting results of FT-IR of YW coal samples.

of the YW coal sample under different temperatures. It can be seen that the adsorption capacity of methane increases significantly with increasing the pressure under the same temperature. This phenomenon demonstrates that it is conductive to the adsorption of methane under higher-pressure conditions. With increasing temperature, the methane adsorption amount is significantly weakened. At the pressure of 7.0 MPa, the methane adsorption capacity of the YW coal sample is 28.5 cm^3/g under the temperature of 20°C. Comparably, the methane adsorption amount under the temperature of 100°C is only 15.9 cm^3/g, decreasing by 44%. At the pressure of 1 MPa, with the temperature increases from 20°C to 100°C, the methane adsorption amount decreases from 10.0 cm^3/g to 7.1 cm^3/g.

3.5. Simulation of Methane Adsorption in Micropores of Coal Sample. The pores of the model are calculated based on the 3D YW coal molecule, as shown in Figure 5. It can be seen from there are many pores in the coal matrix. These pores are very small in size, and the pore size ranges from 0.34 to 1.0 nm. In addition, the shape of these micropores is irregular. We employed methane adsorption simulation by using the 3D YW coal molecule and these methane molecules are adsorbed in the micropore (Figure 5). Figures 6(a) and 6(b) illustrate the simulation adsorption capacity of methane under different pressures and temperatures. With the methane pressure increasing from 1 MPa to 7 MPa at 100°C, the absolute adsorption amount of methane increases from 7.52 cm^3/g to 14.50 cm^3/g, and the excess adsorption amount of methane increases from 7.30 cm^3/g to 12.91 cm^3/g. While, when the pressure reaches critical value, the absolute adsorption amount is found saturated, then the excess adsorption amount will show downward trend. Compared with pressure, temperature has a negative effect on methane adsorption. With temperature increasing, the adsorption capacity of methane gradually decreases. When the temperature is 20°C, the absolute methane adsorption amount and excess methane adsorption amount is 25.2 cm^3/g and 23.0 cm^3/g under 7 MPa pressure. When the temperature increases to 100°C, the absolute methane adsorption amount and excess methane adsorption amount decreases from 14.50 cm^3/g to 12.91 cm^3/g at 7 MPa pressure, decreasing by 42.4% and 43.9%, respectively.

3.6. Simulation Methane Adsorption in Mesoporous. Figures 7(a) and 7(b) demonstrated the simulation results of the methane adsorption behavior in mesopores. When the temperature increases, the methane adsorption capacity

Table 3: Regional content of aromatic hydrocarbons (the assignments of the FT-IR is according to [37]).

Chemical shift (cm^{-1})	Relative area (%)	Peak position attribution
720	1.79	Skeleton vibration of (CH_2) $n \circ > 4$ on the side chain of n-alkanes
748	11.28	Out of plane deformation vibration of CH in aromatics (4-5 adjacent H atoms)
771	12.29	
790	26.87	
804	9.24	Out of plane deformation vibration of CH in aromatics (3 adjacent H atoms)
822	20.48	
834	4.14	
860	2.34	Out of plane deformation vibration of CH in aromatics (2 adjacent H atoms)
875	1.51	
890	9.43	

Table 4: Regional content of oxygen-containing functional groups (the assignments of the FT-IR is according to [37]).

Chemical shift (cm^{-1})	Relative area (%)	Peak position attribution
1012	0.77	C-O-C telescopic vibration
1031	4.54	
1055	3.72	
1078	3.95	
1099	5.22	C-O-C symmetric telescopic vibration
1120	6.11	
1164	6.14	R-O-C telescopic vibration
1202	0.46	Ar-O-C telescopic vibration
1316	0.92	
1344	2.02	
1369	2.16	CH_3 symmetrical bending vibration
1385	2.28	
1402	4.91	
1427	3.13	Asymmetric deformation vibration of CH_3 and CH_2
1459	0.20	
1500	1.06	
1520	4.07	
1547	37.83	Aromatics C°=°C skeleton vibration
1580	1.77	
1631	2.06	
1692	0.33	Stretching vibration of C°=°O in quinone and anhydride
1738	6.36	

Table 5: Regional content of aliphatic carbon (the assignments of the FT-IR is according to [37]).

Chemical shift (cm^{-1})	Relative area (%)	Peak position attribution
2836	5.37	CH_2 telescopic vibration
2853	11.92	CH_3 telescopic vibration
2870	23.69	
2899	26.00	CH telescopic vibration
2924	14.99	CH_2 asymmetric telescopic vibration
2942	6.86	
2963	11.18	CH_3 asymmetric telescopic vibration

Table 6: Regional content of hydroxyl group (the assignments of the FT-IR is according to [37]).

Chemical shift (cm^{-1})	Relative area (%)	Peak position attribution
3197	5.14	Ring stretching vibration
3295	21.28	OH-O stretching vibration
3385	20.72	OH-OH stretching vibration
3461	46.97	
3544	5.90	OH-Π telescopic vibration

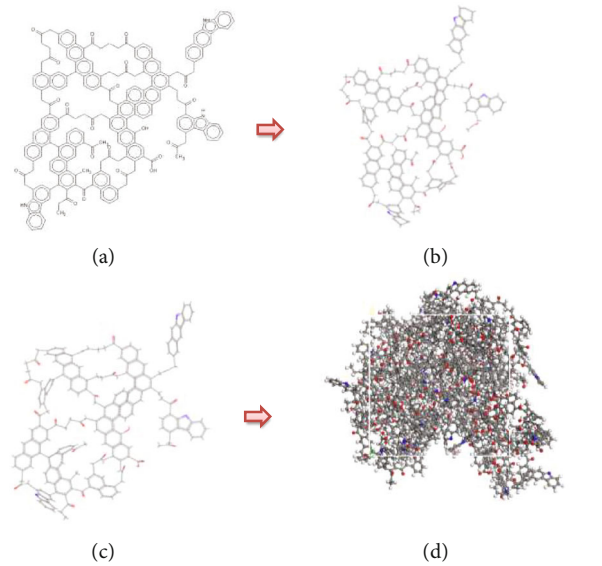

Figure 3: Molecular structure model of YW anthracite. ((a) 2D molecular model; (b) 3D structure optimization results; (c) 3D structure after anneal treatment; (d) 3D molecule structure with 14 molecules).

decreases significantly in 3°nm pore. This phenomenon is consistent with the adsorption of methane in micropores and experimental data. With pressure increasing from 1°MPa to 7°MPa at temperature of 100°C, the absolute adsorption amount of methane increases from $6.23 \times 10^{-3} \circ cm^3/g$ to $4 \times 10^{-2} \circ cm^3/g$, and the excess adsorption amount of methane increases from $2.70 \times 10^{-3} \circ cm^3/g$ to $1.43 \times 10^{-2} \circ cm^3/g$, respectively. When temperature increases from 20°C to 100°C, the absolute adsorption amount of methane decreases from $6.6 \times 10^{-2} \circ cm^3/g$ to $4 \times 10^{-2} \circ cm^3/g$, and the excess adsorption amount of methane decreases from $2.98 \times 10^{-2} \circ cm^3/g$ to $1.43 \times 10^{-2} \circ cm^3/g$ under 7°MPa pressure. With the temperature rising from 20°C to 100°C, the absolute adsorption amount and excess adsorption amount decreases by 33.33% and 52.01%, respectively (at 7°MPa pressure).

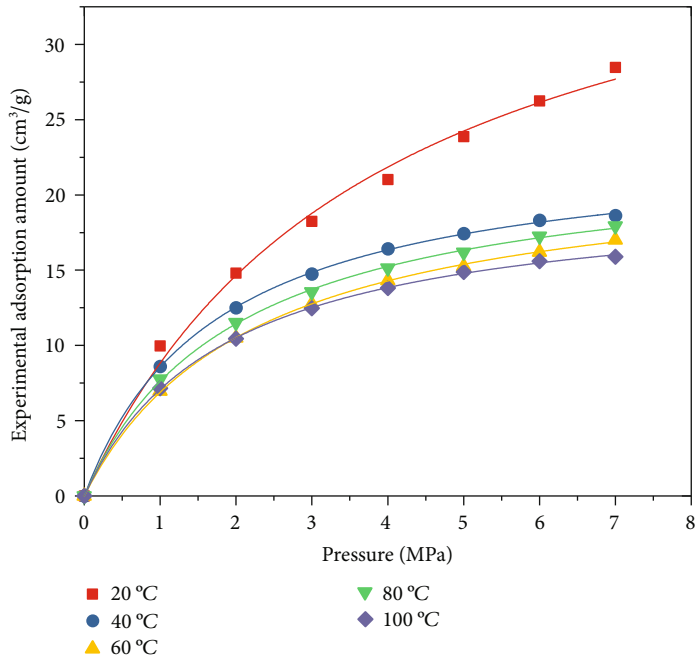

Figure 4: Experimental methane adsorption isothermal data of YW coal samples under different temperatures.

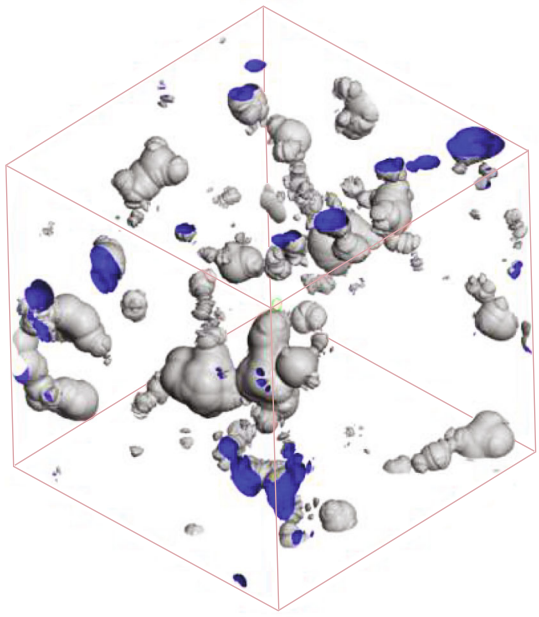

Figure 5: Pore distribution in YW anthracite coal molecule (3.345 nm × 3.345 nm × 3.345 nm).

4. Discussion

4.1. Methane Adsorption Density at Different Pressure and Temperature. Figures 8(a) and 8(b) show the methane density distribution in 3 nm pores under different temperature and pressure. The adsorbed methane molecule is mainly located near the pore walls, and the methane adsorption density near the pore surface is much larger than that in the center of the slit pore. In addition, the methane density in the center of slit pore increases linearly with increasing the pressure. The density of adsorbed layers near the pore wall firstly increases significantly, and then increases slowly when the pressure is larger than 4 MPa. Figure 8(b) shows the methane density distribution at different temperatures. It can be found that with increasing the temperature, the methane density near the pore walls and in the center of the pore both decreases. However, the decrease of methane density in the center of pore is not obvious with increasing the temperature. Comparably, the methane density on the pore surface decreases significantly. It indicates that the temperature significantly affects adsorbed methane molecules. In Figures 8(a) and 8(b), the density near the pore surface is more sensitive to the pressure and temperate compared to the methane in the center of the pores. In addition, it can be seen that as the pressure increases, the methane density on both sides of the pore wall increases. While, as the temperature increases, the density of methane on both sides of the pore decreases. The reason is that the pores provide enough space in anthracite coal molecules, and as the pressure increases, more methane will be adsorbed on the pore surface. However, as the temperature increases, the methane molecules adsorb thermal energy and convert it into kinetic energy, thereby breaking the adsorption force of the pore wall and escaping from the pores. These simulation results are consistent with the experimental results of methane adsorption isotherm.

4.2. The Effect of Temperature on Methane Adsorption Amount of Coal. Figure 9 shows the experimental methane adsorption data at different temperature. It can be seen that the methane adsorption amount of coal sample at 20°C is significantly larger than those at larger temperature. Based

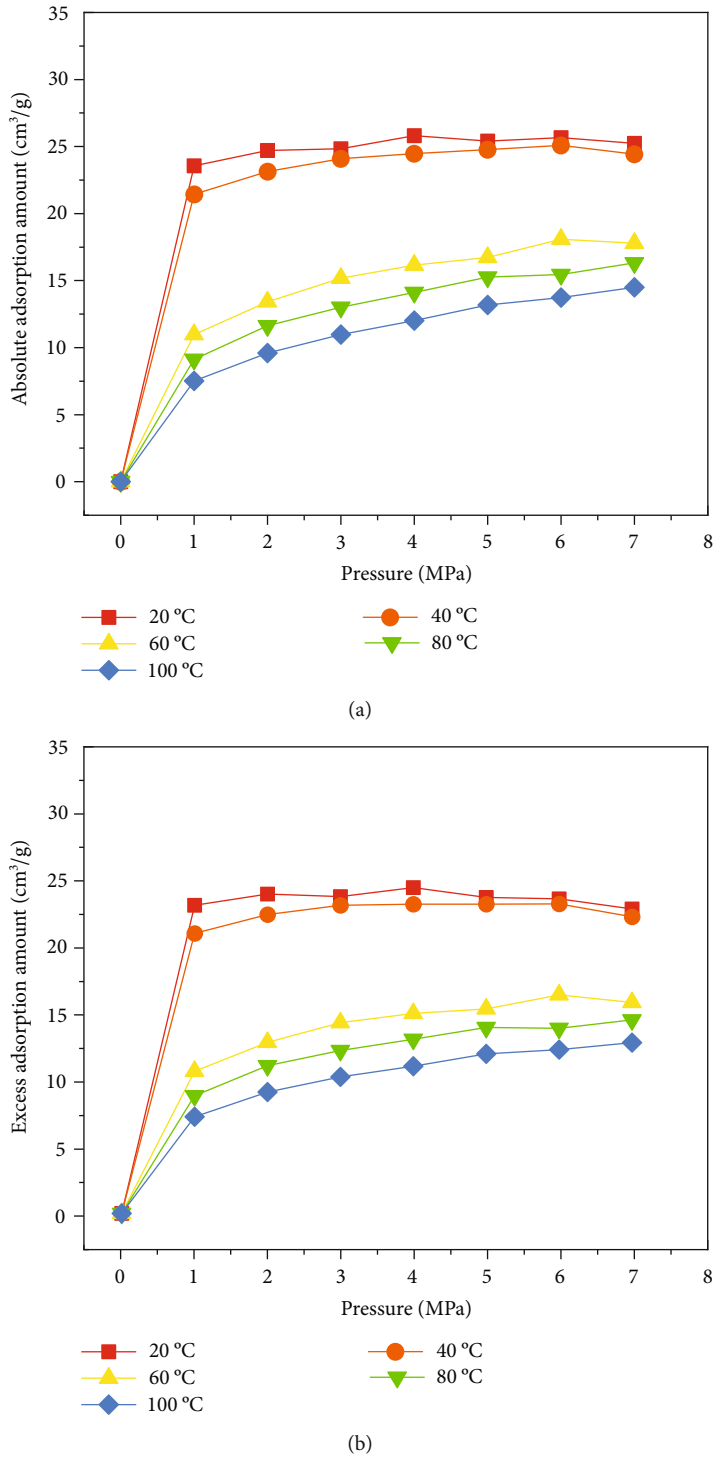

Figure 6: Simulation methane adsorption under different temperatures ((a) absolute adsorption amount under different temperatures; (b) excess adsorption amount under different temperatures).

on Figure 9, it can be seen that when the pressure is larger, the temperature has larger effect on the methane adsorption amount. At 7 MPa, the methane adsorption amount is 28.5 cm^3/g under 20°C, and decreases to 15.9 cm^3/g under 100°C, decreasing by 44%. However, at 1 MPa, the methane adsorption amount is 10.0 cm^3/g under 20°C, and decreases to 7.1 cm^3/g under 100°C, decreasing by 28%.

Experimental data illustrate the overall methane adsorption amount in all pores of coal sample including micropores, mesopores, and macropores. As shown in Figures 6 and 7, methane adsorption in micropores is different from that in mesopores. Thus, it should be discussed separately. Figure 10 shows the relationship of temperature and methane adsorption amount in micropores under different

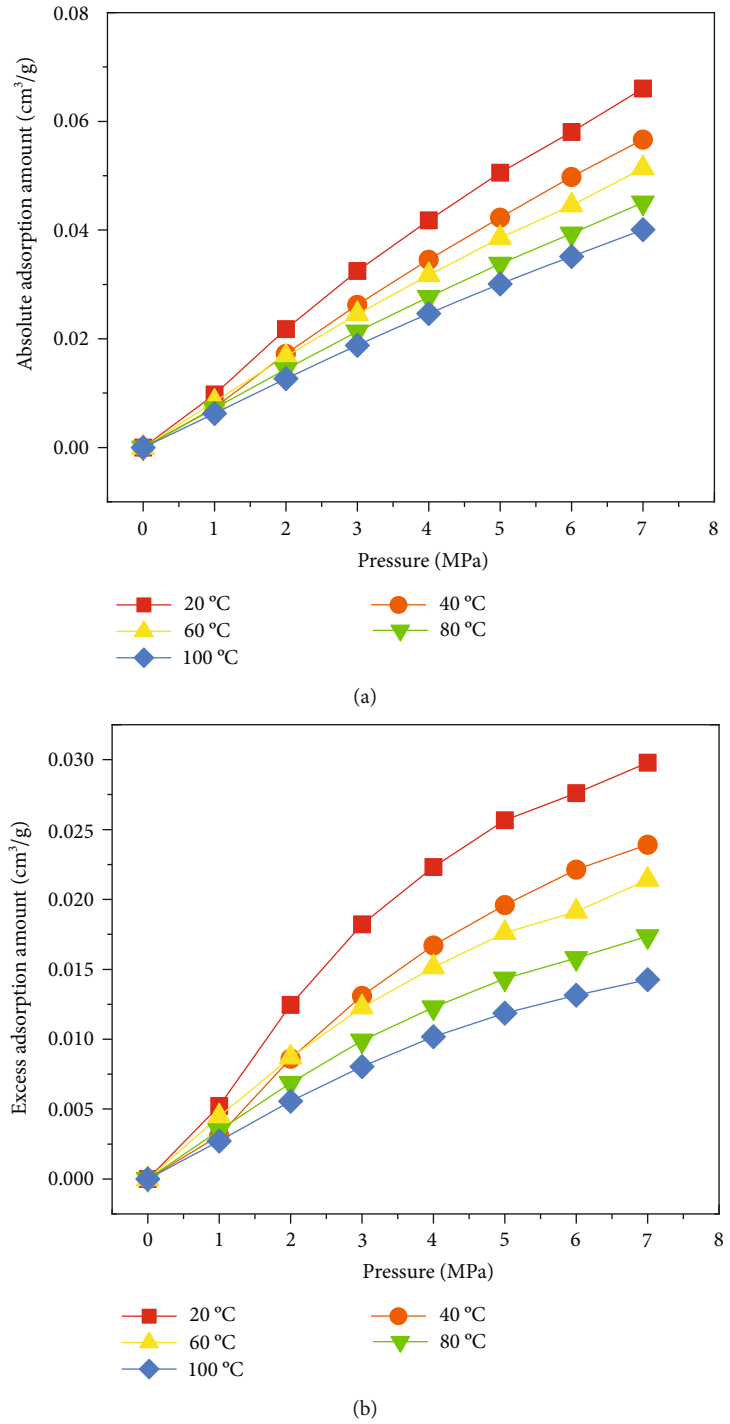

Figure 7: Simulation methane adsorption in 3 nm pore under different temperatures (a) absolute adsorption amount under different temperatures; (b) excess adsorption amount under different temperatures).

pressure. It can be found that at 20°C the adsorption amount in micropores at different pressure is similar, but at 100°C, the methane adsorption amount is micropores at lower pressure is obviously smaller than that at high pressure. It means, in micropores, temperature have larger effects on methane adsorption at low pressure than that at high pressure.

Figure 11 shows the influence of temperature on methane adsorption in mesopores under different pressure. With increasing the temperature, the methane adsorption amount decreases, which is consistent to the experimental data (Figure 9). It is also obvious that temperature has larger effect on methane adsorption amount at higher pressure than that at lower pressure. At 1 MPa, the

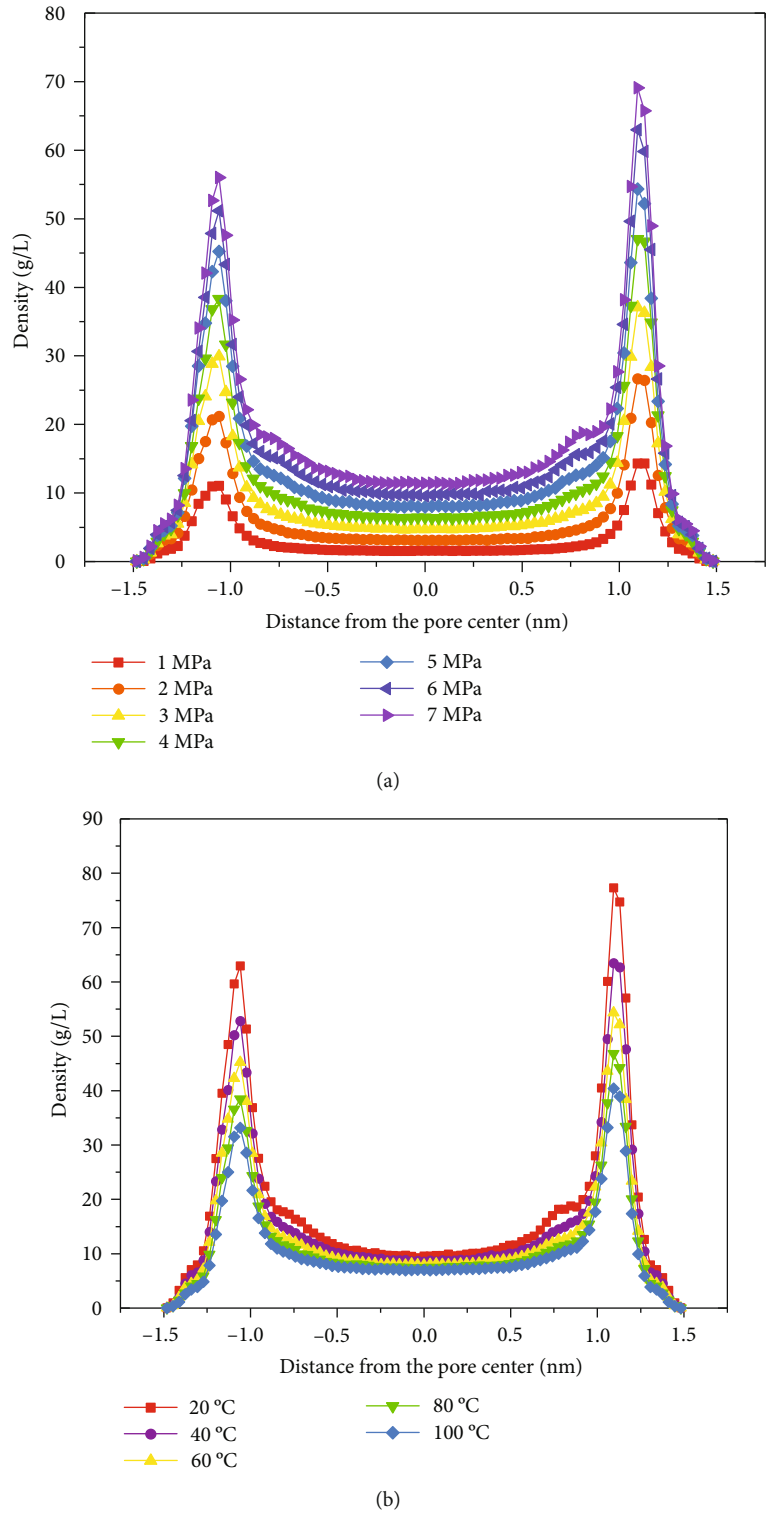

Figure 8: Characteristics of methane density variation in 3 nm slit pore at different pressures (a) and different temperatures (b).

methane adsorption amount at 20°C is 0.01 cm^3/g, and decreases to 0.0027 cm^3/g at 100°C, decreasing by 48%. Comparably, at 7 MPa, the methane adsorption amount at 20°C is 0.066 cm^3/g, and decreases to 0.014 cm^3/g at 100°C, decreasing by 78%. By comprehensively analyzing that the methane behavior in micropore, mesopore, and macropores, when the pressure is higher, temperature has larger effects on methane adsorption in mesopores and macropores, and has weaker effects on methane adsorption in micropores. The experimental data show

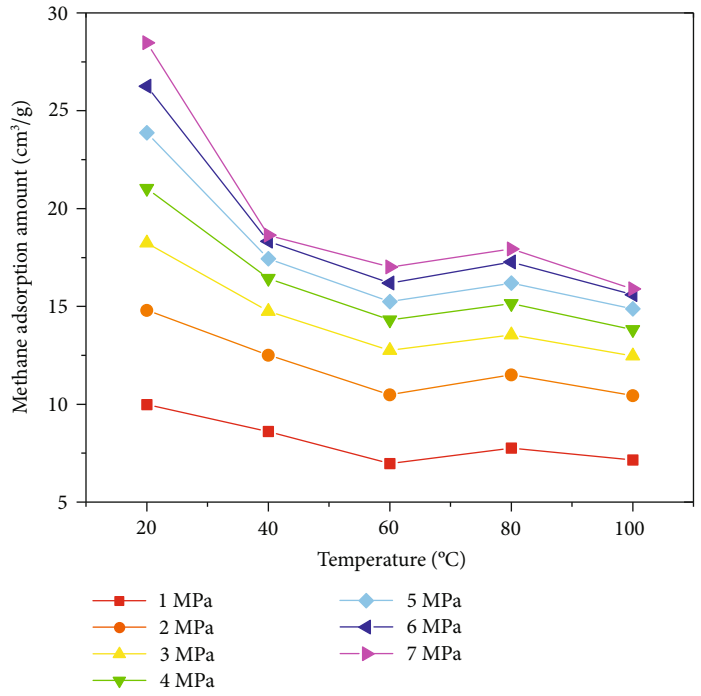

Figure 9: The effect of temperature on methane adsorption amount of coal (experimental data).

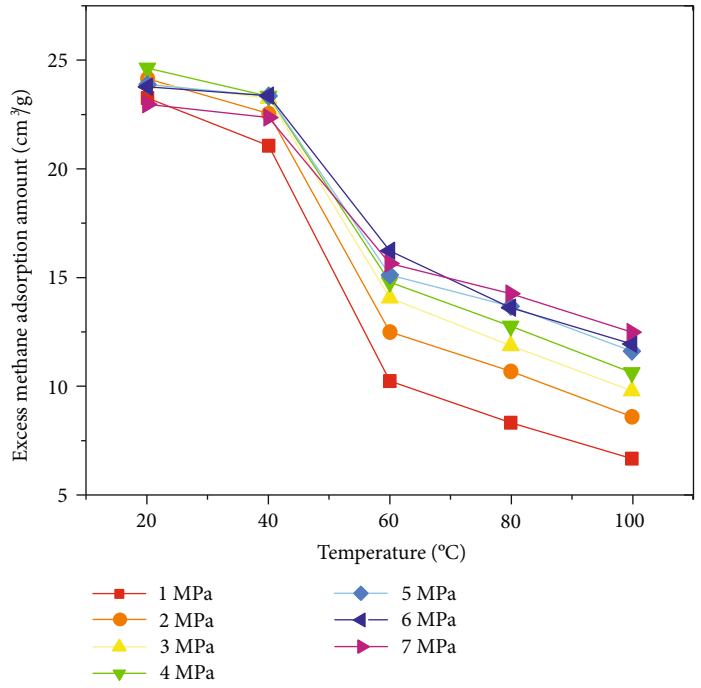

Figure 10: The effect of temperature on methane adsorption amount in micropores (simulation data).

that in YW coal sample, the temperature has larger effects on methane adsorption methane adsorption at high-pressure stage, which is consistent to the phenomenon of methane adsorption in mesopore and macropores, and is contrary to the phenomenon of methane adsorption in micropore. It indicates that the mesopores and macropores in YW coal sample finally determine the temperature effect on methane adsorption.

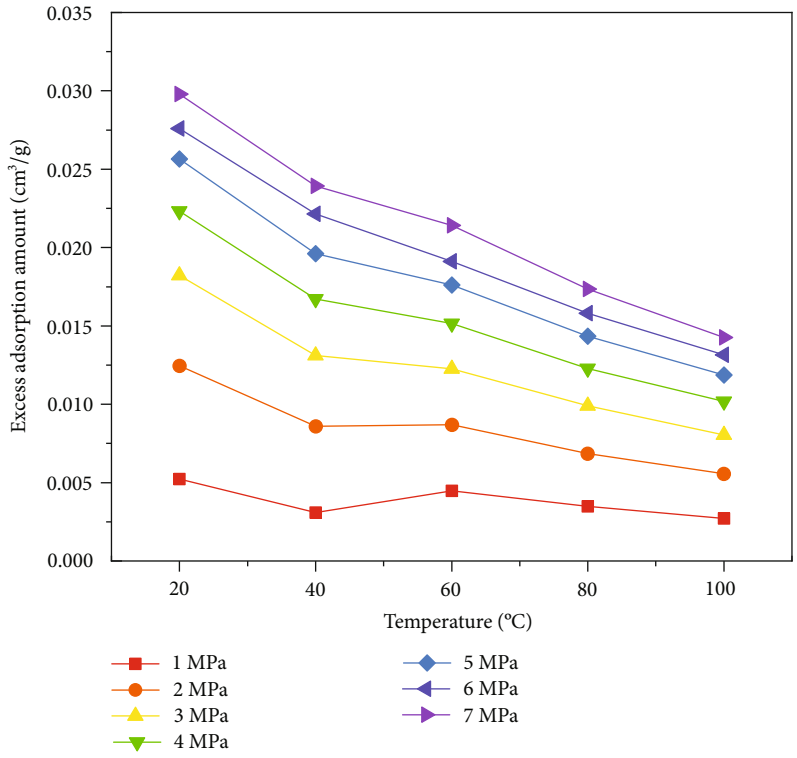

Figure 11: The effect of temperature on methane adsorption amount in mesopores (simulation data).

5. Conclusions

(1) Based on the ^{13}C NMR data and FT-IR data, the carbon skeleton of YW coal sample is mainly composed by aromatic carbon structure (72%), followed by aliphatic carbon structure (14.2%). Carbons connected to the oxygen atoms contribute 13.7% of the total carbons in coal molecule, and the oxygen atoms mainly exit in the form of carbonyl

(2) The average chemical formula of the coal molecule is $C_{200}H_{133}O_{21}N_3$ and the nitrogen atoms are in the form of pyrrole rings. By combining 14 coal molecules, the 3D macromolecular model was built and the size of the 3D macromolecular model is 3.345 nm × 3.345 nm × 3.345 nm

(3) The experimental methane adsorption isothermal data of the YW coal sample under different temperatures show that with increasing the temperature, the methane adsorption amount decreased obviously. At 7 MPa, the methane adsorption amount of the YW coal sample is 28.5 cm^3/g under 20°C. Comparably, less than 100°C and 2 MPa, the methane adsorption amount is only 15.9 cm^3/g, and decreases by 44%. Besides, the experimental data show that in YW coal sample, the temperature has larger effects on methane adsorption methane adsorption at higher pressure stage

(4) In mesopores and macropores, temperature has larger effects on methane adsorption at higher pressure than that at lower pressure. On the contrary, in micropores, temperature has weaker effects on methane adsorption at higher pressure than that at lower pressure

Data Availability

The data used to support the findings of this study are included within the article.

Conflicts of Interest

The authors declare that there are no conflicts of interest.

Acknowledgments

The authors would like to thank Mining Branch of Huaneng Yunnan Diandong Energy Co., Ltd. for their help to offer the cores. This research was funded by China Huaneng Group High-Level Talents Programme (Research on Spatial Distribution and Control Technology of Methane in Yunnan Diandong Mining Area), China Huaneng Group Science and Technology Projects (No. HNKJ21-H51, HNKJ21-H67, HNKJ22-H10), Beijing Science and Technology Plan (No. Z201100004520028), National Natural Science Foundations of China (No. 41972123), and National Key Research and Development Program (Project No. 2019YFE0100100). The authors are also very grateful to Postdoc Zhang Yu in Department of Energy and Power Engineering, Tsinghua University, for accessing the simulation software.

References

[1] M. H. Plumlee, J. F. Debroux, T. Dawn et al., "Coalbed methane produced water screening tool for treatment technology and beneficial use," *Journal of Unconventional Oil and Gas Resources*, vol. 5, pp. 22–34, 2014.

[2] Y. Li, C. Zhang, D. Tang, Q. Gan, X. Niu, and R. Shen, "Coal pore size distributions controlled by the coalification process: an experimental study of coals from the Junggar, Ordos and Qinshui basins in China," *Fuel*, vol. 206, pp. 352–363, 2017.

[3] Y. Li, S. Pan, S. Ning, L. Shao, Z. Jing, and Z. Wang, "Coal measure metallogeny: metallogenic system and implication for resource and environment," *Science China Earth Sciences*, vol. 65, no. 7, pp. 1211–1228, 2022.

[4] S. D. Chen, S. Tao, W. G. Tian, D. Z. Tang, B. Zhang, and P. C. Liu, "Hydrogeological control on the accumulation and production of coalbed methane in the Anze block, southern Qinshui basin, China," *Journal of Petroleum Science and Engineering*, vol. 198, p. 108138, 2021.

[5] S. Tamamura, T. Murakami, A. Ueno et al., "Formation of coalbed methane and water-dissolved gas in Kushiro Coal Mine, Japan, based on isotopic compositions of gas, groundwater, and calcite," *International Journal of Coal Geology*, vol. 229, p. 103577, 2020.

[6] P. J. Crosdale, B. B. Beamish, and M. Valix, "Coalbed methane sorption related to coal composition," *International Journal of Coal Geology*, vol. 35, no. 1–4, pp. 147–158, 1998.

[7] Y. Li, J. Yang, Z. Pan, S. Meng, K. Wang, and X. Niu, "Unconventional natural gas accumulations in stacked deposits: a discussion of upper Paleozoic coal-bearing strata in the east margin of the Ordos Basin, China," *Acta Geologica Sinica (English Edition)*, vol. 93, no. 1, pp. 111–129, 2019.

[8] Y. Li, J. Yang, Z. Pan, and W. Tong, "Nanoscale pore structure and mechanical property analysis of coal: an insight combining AFM and SEM images," *Fuel*, vol. 260, p. 116352, 2020.

[9] K. Jian, X. Fu, Y. Ding, H. Wang, and T. Li, "Characteristics of pores and methane adsorption of low-rank coal in China," *Journal of Natural Gas Science and Engineering*, vol. 27, pp. 207–218, 2015.

[10] H. H. Hou, L. Y. Shao, Y. H. Li et al., "Influence of coal petrology on methane adsorption capacity of the Middle Jurassic coal in the Yuqia coalfield, northern Qaidam Basin, China," *Journal of Petroleum Science and Engineering*, vol. 149, pp. 218–227, 2017.

[11] Z. Pan and D. A. Wood, "Coalbed methane (CBM) exploration, reservoir characterisation, production, and modelling: a collection of published research (2009-2015)," *Journal of Natural Gas Science and Engineering*, vol. 26, pp. 1472–1484, 2015.

[12] Y. Li, Z. Wang, S. Tang, and D. Elsworth, "Re-evaluating adsorbed and free methane content in coal and its ad- and desorption processes analysis," *Chemical Engineering Journal*, vol. 428, article 131946, 2022.

[13] K. Mosher, J. He, Y. Liu, E. Rupp, and J. Wilcox, "Molecular simulation of methane adsorption in micro- and mesoporous carbons with applications to coal and gas shale systems," *International Journal of Coal Geology*, vol. 109-110, pp. 36–44, 2013.

[14] H. Y. Hu, T. W. Zhang, J. D. Wiggins-Camacho, G. S. Ellis, M. D. Lewan, and X. L. Zhang, "Experimental investigation of changes in methane adsorption of bitumen-free Woodford shale with thermal maturation induced by hydrous pyrolysis," *Marine and Petroleum Geology*, vol. 59, pp. 114–128, 2015.

[15] J. H. Levy, S. J. Day, and J. S. Killingley, "Methane capacities of Bowen Basin coals related to coal properties," *Fuel*, vol. 76, no. 9, pp. 813–819, 1997.

[16] B. Ryan and T. Gentzis, "Controls on methane adsorption capacity of lower cretaceous coals from northeastern British Columbia, Canada: part 2-effect of temperature, pressure," *Maceral Composition, and Mineral Matter on Adsorption*, vol. 25, no. 12, pp. 1155–1170, 2003.

[17] L. W. Zhong and X. M. Zhang, "The relationship between methane adsorption capacity and the rank and composition of coal," *Coal Geology & Exploration*, no. 4, p. 29–36+71–74, 1990.

[18] D. Zhao, Y. S. Zhao, Z. C. Feng, Z. X. Liu, and T. Liu, "Experiments of methane adsorption on raw coal at 30-270°C," *Energy Sources, Part A: Recovery, Utilization, and Environmental Effects*, vol. 34, no. 4, pp. 324–331, 2011.

[19] Y. Zhao, Y. Sun, S. Liu, K. Wang, and Y. Jiang, "Pore structure characterization of coal by NMR cryoporometry," *Fuel*, vol. 190, pp. 359–369, 2017.

[20] X. X. He, Y. P. Cheng, B. Hu et al., "Effects of coal pore structure on methane–coal sorption hysteresis: an experimental investigation based on fractal analysis and hysteresis evaluation," *Fuel*, vol. 269, p. 117438, 2020.

[21] B. Hu, Y. P. Cheng, X. X. He, Z. Y. Wang, Z. N. Jiang et al., "New insights into the CH4 adsorption capacity of coal based on microscopic pore properties," *Fuel*, vol. 262, article 116675, 2020.

[22] F. An, Y. Cheng, D. Wu, and L. Wang, "The effect of small micropores on methane adsorption of coals from northern China," *Adsorption*, vol. 19, no. 1, pp. 83–90, 2013.

[23] S. Wu, D. Tang, S. Li, H. Chen, and H. Wu, "Coalbed methane adsorption behavior and its energy variation features under supercritical pressure and temperature conditions," *Journal of Petroleum Science and Engineering*, vol. 146, pp. 726–734, 2016.

[24] C. J. Liu, S. X. Sang, X. F. Fan et al., "Influences of pressures and temperatures on pore structures of different rank coals during CO_2 geological storage process," *Fuel*, vol. 259, p. 116273, 2020.

[25] M. S. A. Perera, P. G. Ranjith, S. K. Choi, D. Airey, and P. Weniger, "Estimation of gas adsorption capacity in coal: a review and an analytical study," *Estimation of Gas Adsorption Capacity in Coal: A Review and an Analytical Study. International Journal of Coal Preparation and Utilization*, vol. 32, no. 1, pp. 25–55, 2012.

[26] G. Yue, Z. Wang, X. Tang, H. Li, and C. Xie, "Physical simulation of temperature influence on methane sorption and kinetics in coal (II): temperature evolvement during methane adsorption in coal measurement and modeling," *Energy & Fuels*, vol. 29, no. 10, pp. 6355–6362, 2015.

[27] L. Zhong, "Adsorptive capacity of coals and its af fecting factors," *Earth Science*, vol. 29, no. 3, p. 327-332+368, 2004.

[28] J. Shen, Y. Qin, X. H. Fu, G. Wang, R. Chen, and L. J. Zhao, "Study of high-pressure sorption of methane on Chinese coals of different rank," *Arabian Journal of Geosciences*, vol. 8, no. 6, pp. 3451–3460, 2015.

[29] Y. Qin, T. A. Moore, J. Shen, Z. B. Yang, Y. L. Shen, and G. Wang, "Resources and geology of coalbed methane in China: a review," *International Geology Review*, vol. 60, no. 5–6, pp. 777–812, 2018.

[30] J. You, L. Tian, C. Zhang et al., "Adsorption behavior of carbon dioxide and methane in bituminous coal: a molecular simulation study," *Chinese Journal of Chemical Engineering*, vol. 24, no. 9, pp. 1275–1282, 2016.

[31] K. Dong, F. Zeng, J. Jia, C. Chen, and Z. Gong, "Molecular simulation of the preferential adsorption of CH4and CO2in middle-rank coal," *Molecular Simulation*, vol. 45, no. 1, pp. 15–25, 2019.

[32] S. Yu, Z. Yan-ming, and L. Wu, "Macromolecule simulation and CH4 adsorption mechanism of coal vitrinite," *Applied Surface Science*, vol. 396, pp. 291–302, 2017.

[33] J. Xiang, F. Zeng, H. Liang, B. Li, and X. Song, "Molecular simulation of the CH4/CO2/H2O adsorption onto the molecular structure of coal," *Science China Earth Sciences*, vol. 57, no. 8, pp. 1749–1759, 2014.

[34] J. Zhang, K. Liu, M. B. Clennell, D. N. Dewhurst, and M. Pervukhina, "Molecular simulation of CO_2-CH_4 competitive adsorption and induced coal swelling," *Fuel*, vol. 160, pp. 309–317, 2015.

[35] A. Marzec, "Towards an understanding of the coal structure: a review," *Fuel Processing Technology*, vol. 77-78, pp. 25–32, 2002.

[36] Y. Liu, S. Liu, R. Zhang, and Y. Zhang, "The molecular model of Marcellus shale kerogen: experimental characterization and structure reconstruction," *International Journal of Coal Geology*, vol. 246, p. 103833, 2021.

[37] P. C. Painter, R. W. Snyder, M. Starsinic, M. M. Coleman, D. W. Kuehn, and A. Davis, "Concerning the application of FT-IR to the study of coal: a critical assessment of band assignments and the application of spectral analysis programs," *Applied Spectroscopy*, vol. 35, no. 5, pp. 475–485, 1981.

[38] J. H. Xiang, F. Zeng, B. Li, and L. Zhang, "Construction of macromolecular structural model of anthracite from Chengzhuang coal mine and its molecular simulation," *Journal of Fuel Chemistry and Technology*, vol. 41, no. 4, pp. 391–400, 2013.

[39] Y. Liu, Y. Zhu, W. Li, C. Zhang, and Y. Wang, "Ultra micropores in macromolecular structure of subbituminous coal vitrinite," *Fuel*, vol. 210, pp. 298–306, 2017.

[40] B. Erdenetsogt, I. Lee, S. K. Lee, Y. Ko, and D. Bat-Erdene, "Solid-state C-13 CP/MAS NMR study of Baganuur coal, Mongolia: oxygen-loss during coalification from lignite to subbituminous rank," *International Journal of Coal Geology*, vol. 82, no. 1–2, pp. 37–44, 2010.

[41] S. Wang, Y. Tang, H. H. Schobert, Y. N. Guo, and Y. Su, "FTIR and13C NMR investigation of coal component of late Permian coals from southern China," *Energy & Fuels*, vol. 25, no. 12, pp. 5672–5677, 2011.